Journal of Alloys and Compounds 505 (2010) 54–63

Contents lists available at ScienceDirect

Journal of Alloys and Compounds

journal homepage: www.elsevier.com/locate/jallcom

The effect of small addition of tin and indium on the corrosion behavior of aluminium in chloride solution

S. Gudić*, I. Smoljko, M. Kliškić

Department of Electrochemistry and Materials Protection, Faculty of Chemistry and Technology, Teslina 10/V, 21000 Split, Croatia

ARTICLE INFO

Article history:
Received 9 November 2009
Received in revised form 6 June 2010
Accepted 8 June 2010
Available online 18 June 2010

Keywords:
Aluminium
Aluminium alloys
Chloride
Corrosion
Hydrogen evolution
Impedance spectroscopy

ABSTRACT

The corrosion behavior of Al, Al–In, Al–Sn and Al–Sn–In alloys in 2 M NaCl solution has been studied by using potentiodynamic polarization, open circuit potential and impedance measurements as well as volumetric determination of evolved hydrogen. Polarization measurements indicated that the alloying elements considerably change the electrochemical behavior of aluminium. Changes are especially pronounced in the anodic branch of the polarization curve, and manifest in significant shift of the corrosion and the pitting potentials in the negative direction, reducing the passive potential region, and increasing the current output already at low anodic overpotentials. The open circuit corrosion process of tested samples was monitored through the period of 17 days. It was established that the dissolution of Al and its alloys is mainly accompanied by the cathodic reaction of hydrogen evolution, with In inhibits the cathodic reaction of hydrogen evolution, while Sn catalyzes the same one. The impedance measurement performed also during the 17 days of corrosion test, provided a continuous monitoring of the parameters, which characterize the properties of the surface and their changes as corrosion occurs. Different equivalent circuits were employed to account for the electrochemical processes taking place at different stages of corrosion.

1. Introduction

The low atomic mass of aluminium, and its high energetic capacity (2980 Ah kg^{-1}), along with the negative value of standard electrode potential (−1.66 V vs. NHE [1]) make the metal potentially attractive as an anode material in Al-batteries and in cathodic protection systems. However, the hindrance for the realization of these theoretical possibilities is the protective oxide film, which is spontaneously formed on Al surface in air and in aqueous solutions. Due to presence of oxide film, the corrosion potential of Al electrode is shifted in the positive direction (almost for 1.0 V), and the active dissolution of Al is slowed down considerably. This causes a significant loss of available energy and makes Al unattractive as energetic anode material.

However, if Al is alloyed with small quantities of elements such as Hg, In, Ga, Zn, Sn and others [2–21], its anodic activity improves as the structure of the aluminium/aluminium oxide film/chloride electrolyte system changes. The activation of Al is manifested by a displacement of the solution potential in the electronegative direction, the system's ability to deliver high anodic current density, and the maintenance of an active surface that corrodes in a nearly uniform manner. In order to make the Al/air batteries or cathodic protection systems more economical, the possibilities of replacement of the special alloys made from super-pure Al with binary or ternary alloys of technical purity have been investigated lately [5,19,20]. Activation of Al can also be achieved by adding small quantities of suitable metal cations, like In^{3+}, Ga^{3+}, Hg^{2+}, Sn^{4+}, Sn^{2+} to the electrolyte [9,15,22–27].

The present paper describes the corrosion behavior of technical grade Al (99.8%) and its alloys Al–0.1%In, Al–0.2%Sn, Al–0.1%In–0.2%Sn in stagnate 2 M NaCl solution. The selection of technical grade Al, its binary alloys and ternary alloy for this study was based on insufficient examination of application of these materials as anode materials in Al/air batteries in which 2 M NaCl is a common used electrolyte. According to our knowledge, no literatures have reported usage of Al–0.2%Sn–0.1%In alloy in this application. This combination of elements taken into consideration is entirely novel. In the available literature electrochemical studies were usually performed on samples of binary alloys of high-purity Al (99.999%) with Sn and In.

The main objective of this work was to detect, measure and monitor corrosion of tested samples. For this purpose, just after immersing the tested electrodes in the solution, the variation of the open circuit potential, volume of the evolved hydrogen, as well as pH value of solution, were measured trough the period of 17 days. Impedance measurements were also performed at various

* Corresponding author.
E-mail address: senka@ktf-split.hr (S. Gudić).

0925-8388/$ – see front matter © 2010 Elsevier B.V. All rights reserved.
doi:10.1016/j.jallcom.2010.06.055

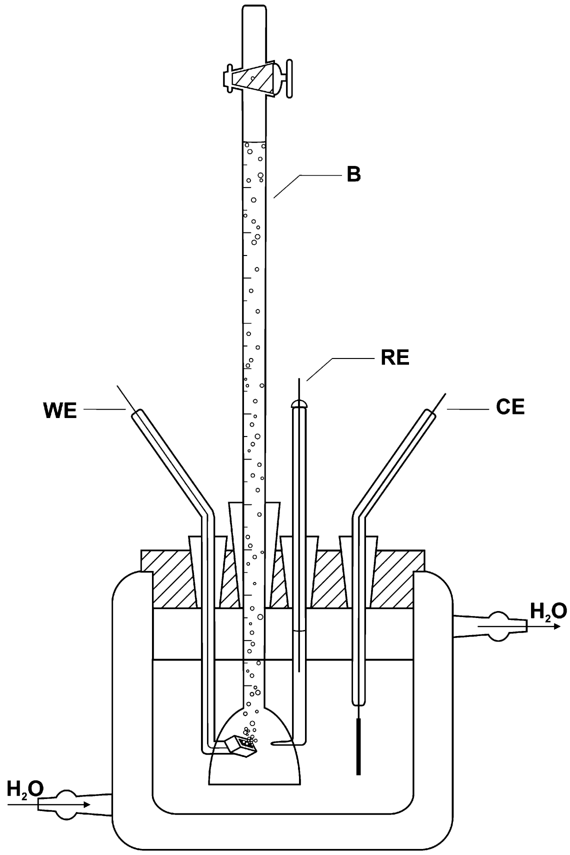

Fig. 1. The electrochemical cell. WE – electrode under test; RE – reference electrode; CE – counter electrode; B – gas burette.

exposure times during the 17 days corrosion test, while the surface damage after the test was observed by optical microscopy. In addition, prior to long term corrosion test, the polarization curves for each sample were recorded in wide potential range.

2. Experimental

The experiments were performed on Al and Al–0.1%In, Al–0.2%Sn, Al–0.1%In–0.2%Sn alloys. The alloys have been prepared with aluminium purity of 99.8% as the primary component, and super-pure tin and indium as the alloying components. After alloying, the metal was homogenized at 800–850 °C for 15 min. The alloys were quenched in cold water.

The examined samples were made into electrodes by inserting insulated copper wire and protecting all sides but one with epoxy resin. The exposed geometric area was 0.5 cm^2. Prior to each measurement the exposed surface was mechanically polished using successively finer grades of emery paper (until a mirror-bright surface was attained), followed by the alkali attack by immersing the electrode for 1 min in 0.1 M NaOH at 40 °C. Then, the electrodes were rinsed in doubly distilled water and placed in the closed Pyrex glass cell shown in Fig. 1, which enabled performances of electrochemical measurement, as well as measurement of hydrogen evolution volume during the corrosion test. The counter electrode was a platinum sheet and the reference electrode was a saturated calomel electrode (SCE). All measurements in this work were carried in freshly prepared (unstirred) 2 M NaCl solution at 25 ± 0.1 °C. The volume of the electrolyte was 200 ml.

The characterization of each sample was started with potentiodynamic polarization measurements. The polarization curves were recorded in the potential range from −2.0 to −0.5 V at a scan rate of 2 mV s^{-1}. After that, the examination of corrosion behavior of samples at open circuit potential followed. For this purpose, just after immersing the tested electrodes in the solution, the variation of the open circuit potential, volume of the evolved hydrogen, as well as pH value of solution were measured trough the period of 17 days. The volume of the evolved hydrogen was determined as follows. After preparation, the tested electrode was placed in the cell under the burette. The electrolyte was sucked to fill the burette. The evolving gas accumulated in the burette, pushed the electrolyte out into the electrolyte. At the end of the measurements, the volume of evolved hydrogen was determined.

The impedance spectra were also recorded at various exposure times during the 17 days corrosion test. The measurements were performed in a wide frequency range, from 100 kHz to 100 mHz, with an ac voltage amplitude of ±5 mV. Data were processed according to the EQUIVCRT program (B.A. Boukamp, University of Twente). The electrochemical measurements were carried out by an EG&G PAR potentiostat/galvanostat model 273A with a lock-in amplifier model 5210 controlled by a computer. After 17 days the surface of Al and Al alloys was observed by an optical microscope Citoval (Carl Zeiss Jena) at magnification of 100 times.

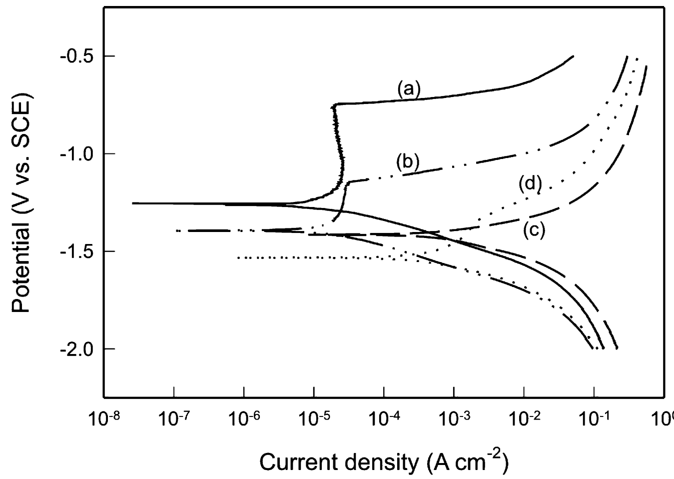

Fig. 2. Potentiodynamic polarization curves of (a) Al, (b) Al–In, (c) Al–Sn and (d) Al–In–Sn electrodes in 2 M NaCl solution.

3. Results and discussion

3.1. Potentiodynamic polarization measurements

Fig. 2 compares the potentiodynamic polarization curves of Al, Al–In, Al–Sn and Al–In–Sn alloys in 2 M NaCl solution. The polarization curve for Al is characterized by a broad passive region over which the current density is constant and relatively small. This passive region is attributed to the formation of protective oxide film on aluminium surface. At the end of the passive region (i.e. at ≈−0.74 V) the current increases abruptly as a consequence of the pitting initiation process and hence the passivity breakdown. The cathodic branch of the polarization curve probably reflected the rate of the hydrogen evolution reaction. This is supported by the experimental finding of the cathodic Tafel slope of ≈−120 mV dec^{-1} near the corrosion potential, which is a characteristic of hydrogen evolution according to the Volmer–Tafel mechanism (−118 mV dec^{-1}) [28].

The polarization measurements indicated that the alloying elements considerably change the electrochemical behavior of aluminium in the same potential range. The changes can be observed in the anodic, but also in the cathodic branch of the polarization curve. For example, the addition of indium to aluminium produced the significant shift of the corrosion and the pitting potentials in the negative direction and reduction of the passive potential region. As can be seen from Fig. 2, after passing the short passive potential range (of only 0.2 V), the Al–In alloy starts to dissolve actively at ≈−1.15 V. Anodic current density increases sharply, and already at −1.0 V becomes about three orders of magnitude higher than the current density on Al (Al remains passive). Moreover, the cathodic part of the current–potential curve was shifted towards lower current, showing that the In reduced the cathodic hydrogen evolution on Al.

On the other hand, the Al–Sn alloy exhibits quite different behavior from that of Al, since the anodic polarization curve shows an active dissolution without any passivity. Namely, the dissolution potential takes a value close to corrosion potential (≈−1.43 V), while the anodic current density increases exponentially with the potential. The cathodic polarization curve was also shifted towards

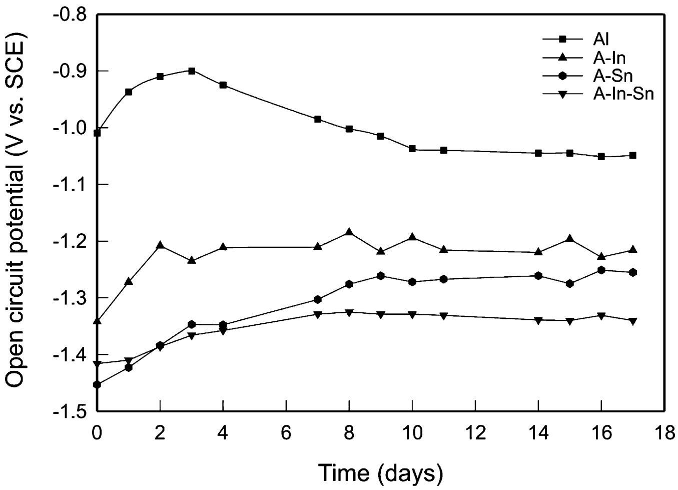

Fig. 3. Variation of the open circuit potential of Al and Al alloys with time in 2 M NaCl solution.

higher currents, showing that the Sn catalyzed the cathodic reaction on Al.

The polarization curve of Al–In–Sn alloy is characterized by a markedly negative value of corrosion potential of −1.53 V and ill defined a small passive region of about 50 mV. Rapid increase in the anodic current at −1.35 V indicates the start of pitting attack. Compare to Al, the cathodic branch of polarization curve is shifted towards lower current.

3.2. Open circuit potential (OCP) and stability to corrosion

Fig. 3 shows the variation of the OCP of Al, Al–In, Al–Sn and Al–In–Sn electrodes during the 17 days of exposure to the NaCl solution. The potential of the Al electrode moves in the positive direction, reaches a maximal value of ≈−0.90 V after 3 days, and than decreases with time. After 17 days the OCP of ≈−1.05 V was achieved. The increase in the open circuit potential with time is known to arise from the growth of the surface oxide film, while the decrease of OCP can be attributed to composite change of oxide film due to incorporation of Cl^- ions [29–31].

As can be seen from Fig. 3, the addition of alloying elements to Al produced in all cases a considerable shift of the OCP in the negative direction. In the beginning, through the first 2 days, the potential of the Al–In electrode shifts in a positive direction. After that, with small oscillations, an average OCP value of ≈−1.22 V was achieved. It is interesting to note that this potential is equal to the potential of active dissolution of Al–In alloy.

As soon as the Al–Sn and Al–In–Sn alloys were immersed in the NaCl solution very negative potentials are measured (−1.45 V for Al–Sn alloy, and −1.42 V for Al–In–Sn alloy). These potentials remained constant during the first few hours, where the active dissolution of electrodes is evident. After that, the potential of both alloys moves in the positive direction, and after 17 days values of ≈−1.26 V and ≈−1.34 V were achieved on Al–Sn and Al–In–Sn alloys, respectively. This enabled potential can be attributed to the passivation of the electrode surface by deposition of corrosion products. But some differences are noticed in manner of alloying elements in binary and ternary alloys influence the Al passivation process at prolonged immersion times.

The significant electrochemical activity imparted by In and Sn on addition to Al is evident from the results of potentiodynamic and open circuit measurements. It is known (from the physical metallurgy and phase diagrams of Al alloys) that In and Sn are negligibly soluble in Al. Sn has been observed to have a solubility of less than 0.01% in the Al matrix at the melting point of 232.2 °C [32], while the solubility of In is 0.017% at the melting point of 156 °C [21,32]. By increasing the temperature the solubility of alloying elements in Al increases; for example the solubility of Sn is approximately 0.1% at 600 °C [32]. Due to low solubility of In and Sn in solid Al the total quantity of alloying elements above the solubility limit at the determined temperature is segregated into inclusions by predominantly at grain boundaries, but also within metal grains [21,32–35].

It is suspected that galvanic cells set up between In(Sn) inclusions and the Al matrix resulting in the local dissolution of Al in the vicinity of the In(Sn), when they are immersed in chloride solution. The consequence of this phenomenon is the local breakdown of the surface film and subsequent local dissolution of the metallic substrate [36–38]. Hence, the presence of heterogeneities in the Al structure may strongly affect the continuity and resistance of the surface oxide layer. The localized attack ordinary initiates and propagates at weak point in oxide layer, i.e. in those zones enriched in alloying element during the solidification process (grain boundaries and intermetallic zones).

The partial anodic reaction occurring at anodic sits (i.e. inside a pit) during the localized corrosion of Al in NaCl solution is:

$$Al \rightarrow Al^{3+} + 3e^- \quad (1)$$

Due to acidity at the anodic sites the hydrogen evolution takes place as a secondary cathodic reaction (in the pit):

$$2H^+ + 2e^- \rightarrow H_2 \uparrow \quad (2)$$

Since the NaCl solution contains a certain amount of dissolved oxygen the possible cathodic reactions at cathodic sits (outside the pits) are hydrogen evolution and/or oxygen reduction:

$$2H_2O + 2e^- \rightarrow H_2 \uparrow + 2OH^- \quad (3)$$

$$O_2 + 2H_2O + 4e^- \rightarrow 4OH^- \quad (4)$$

As a result of cathodic reactions, the concentration of hydroxide ions increases, so the local pH becomes more alkaline. Hydrogen gas results from the partial reaction occurring during localized corrosion inside the pit, as well as from the cathodic reaction on the surface outside the pit (reactions (2) and (3)). Also in this work the evolution of gas bubbles of hydrogen has been observed. So, it could be concluded that the corrosion of aluminium and its alloys is mainly accompanied by the cathodic reaction of hydrogen evolution, which is supported by the experimental findings of the cathodic Tafel slopes of ≈−120 mV dec^{-1}.

In order to determine the effect of alloying elements (In, Sn) addition on dissolution process of Al in NaCl solution, the volume of the evolved hydrogen has been measured during the period of 17 days. After the dissolution test the corroded surfaces were examined by optical microscopy to correlate the dissolution features with the microstructure.

The rate of hydrogen evolution of all the samples submerged in chloride solution varied with time (Fig. 4). Due to the positive value of the corrosion potential, the hydrogen slowly evolves on the electrode of Al, especially through the first 3–4 days. However, with time, aggressive ions penetrate into the oxide film. In such conditions micropitts can be formed on the surface of Al, which cause further evolution of hydrogen. Based on the gradually change of pH of the solution (starting value of pH was 5.38, while the final value, i.e. after 17 days was 6.85) it can be concluded that the volume of hydrogen evolved during the corrosion of Al is given by the sum of reactions (2) and (3). Furthermore, the optical microscopy examination of Al electrode after exposure to NaCl revealed a smooth surface with randomly distributed regular-formed pits (Fig. 5a).

More negative OCP value favours the hydrogen evolution reaction. As seen, the OCP of all alloys are so negative (Fig. 3) that the

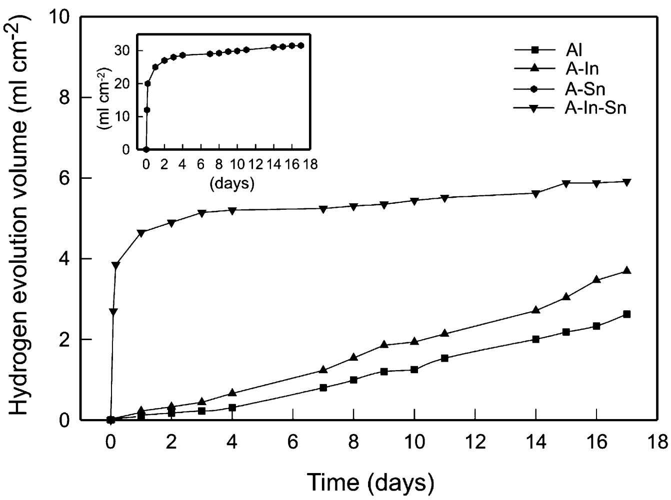

Fig. 4. Volume of evolved hydrogen at Al and Al alloys during the corrosion test in 2 M NaCl solution.

hydrogen is evolved on the entire surface very easy due to electrochemical decomposition of water. At the same time, hydrogen evolution takes place inside pits by the reaction, which is obviously coupled with the Al dissolution. Based on the above, one might expect that hydrogen evolves significantly more on Al alloys than on Al.

On the contrary, the alloy with In exhibited behavior which was comparable to that of Al. Volume of evolved hydrogen is only slightly greater than Al (pH value was 7.57 at the end of measurement). The results obtained can be explained by the fact that In as cathodic inclusion in the alloy inhibits the reaction of hydrogen evolution on Al [24,39–41].

The presence of In as a segregated phase at the grain boundaries or as an In rich phase in the intermetalic zones of the grains promotes higher dissolution rate of Al as well as a higher overpotential for the hydrogen evolution reaction [40]. Both facts shift the corrosion potential of the alloy and its depolarized active potential region towards more negative values. On the other hand, the strong Cl^- adsorption exerted by In on In rich phases or possible surface In–Al alloys brought about by decomposition, promotes its activation at more electronegative potential than corresponding to pure Al [40].

The microstructural observations after treatment in the chloride solution show the strongest attack taking place mainly at the grain boundaries were the In inclusions (the “bright” area) are located (Fig. 5b). Indium inclusions display a cathodic behavior with respect to the Al matrix and hydrogen evolution reaction takes place over these. Acting as cathodic centres, In inclusions support the dissolution of the surrounding Al substrate. The type of attack appears to be typically for inclusions that are electrochemically cathodic to the Al matrix causing preferential dissolution of the matrix. In many cases in literature, traces of indium as “bright” spots were found in pits, over which a slow hydrogen evolution takes place [21,23,24].

Contrary to In, Sn caused a very rapid evolution of hydrogen [20,42,43], and the behavior of Al–Sn alloy differs from the behavior of Al and Al–In alloy during the exposure to the NaCl solution (insert of Fig. 4). After only a few seconds of immersion, the dissolution of metal takes place, accompanied by a violent hydrogen evolution. The Al–Sn electrode became gradually covered by a white film of corrosion products (presumably alumina and/or aluminium hydroxide) and the solution was turned very cloudy at prolonged immersion times. Immediately after these events, all signs of activity dissolution disappear. Namely, the hydrogen evolution leads to the local increase of pH value (with the rapid evolution of hydrogen, pH of the solution increases and after 4 h reaches 8.80), which causes the dissolution of oxide layer according to the reaction:

$$Al_2O_3 + 2OH^-(\text{adsorbed}) \rightarrow 2AlO_2{}^-(\text{aqueous}) + H_2O \quad (5)$$

In parallel, the oxidation of the metal matrix by uniform corrosion is also taking place, and the oxide film is formed, with the physical

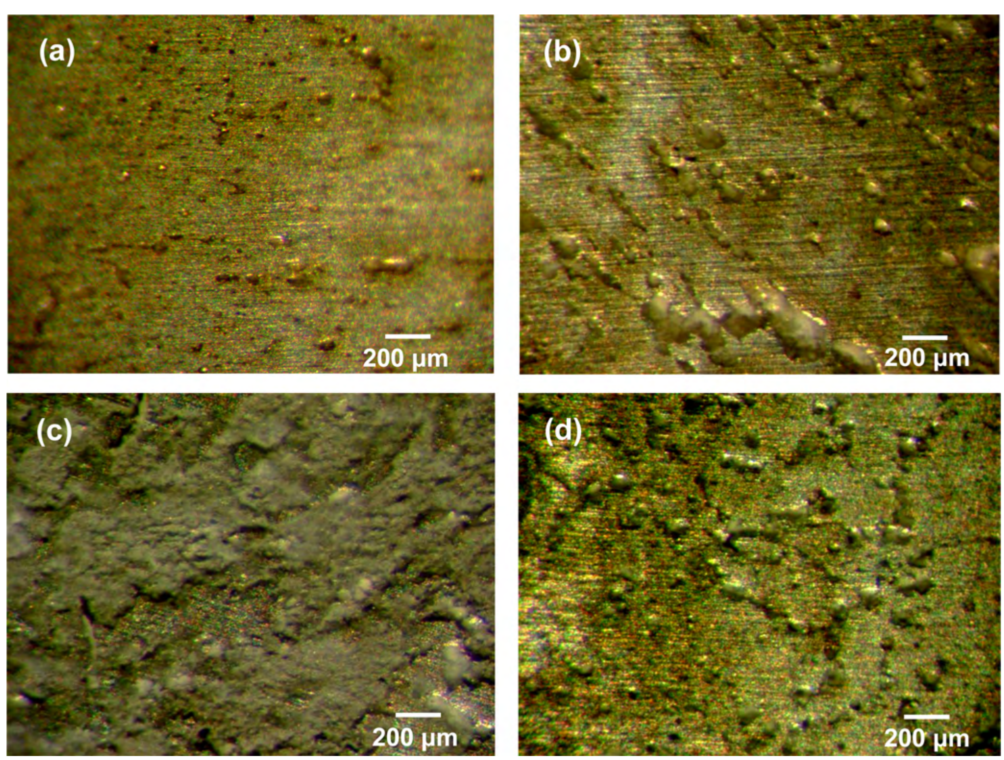

Fig. 5. Corrosion morphology of (a) Al, (b) Al–In, (c) Al–Sn and (d) Al–Sn–In samples obtained after open circuit potential measurement in 2 M NaCl solution for 17 days.

detachment of gaseous hydrogen, according to reaction:

$$2Al + 3H_2O \leftrightarrow Al_2O_3 + 3H_2 \uparrow \quad (6)$$

In this case the accumulation of oxide film on the electrode surface would be the principal factor in reducing Al dissolution, as well as hydrogen evolution by blocking the activation sits. Optical microscopy examination has confirmed that after removing of corrosion products layer, the surface of Al–Sn alloy exhibited rough morphology that is consistent with strong general dissolution (Fig. 5c). Literature data indicate similar behavior of alloys containing small amounts of Sn [20].

Al–In–Sn alloy also exhibited the effect of temporary active dissolution. Results in Fig. 4 demonstrate that as soon as Al–In–Sn alloy is immersed in NaCl solution the hydrogen evolution takes place rapidly (but velocity of reaction is significant lower compare to Al–Sn alloy). At the same time pH of the solution increases and after 4 h was 8.36. However, at longer times of exposure to the chloride solution (i.e., after 24 h) leads to the formation of layers of corrosion products on the surface of the alloy and both the rate of evolution of hydrogen and the pH value of solution reduce.

Due to low solubility of In and Sn in solid Al, during the preparation of Al–In–Sn alloy, there is possibility of extraction of both alloying elements mainly at grain boundary. The contact of In and Sn lead to the formation of new micro-galvanic cells, i.e. a new sources of local corrosion in which In has anodic character in respect to the Sn. Therefore, in the first moments of exposure to chloride solution, the dissolution of Al–In–Sn alloy introduces both Al^{3+} ions (reaction (1)) and In^{3+} ions into the solution:

$$In \rightarrow In^{3+} + 3e^- \quad (7)$$

The anodic reactions are accompanied by strong evolution of hydrogen, which takes place on the top of the Sn inclusions. This in turn produces a local increase in pH, which gives rise to the dissolution of oxide layer (reaction (5)). However, the In species may redeposit on the cathodic sits of the surface, subsequently, and caused the hydrogen evolution decrease:

$$In^{3+} + 3e^- \rightarrow In \quad (8)$$

The exchange current density for the hydrogen evolution reaction on the In is smaller than on Al and Sn. Therefore the In deposition contributes to diminish the hydrogen evolution [24,39]. Furthermore, after producing patches of quasi-bare Al surface (due to oxide dissolution) following reaction can take place:

$$Al + In^{3+} \rightarrow Al^{3+} + In \quad (9)$$

In parallel with the oxidation of the metal matrix the oxide film is formed according to reaction (6), which suppresses further anodic dissolution of alloy.

During the stabilization of Al–In–Sn alloy at OCP following processes simultaneously can takes place: evolution of hydrogen, the dissolution and redeposition of In and dissolution and formation of new oxide film on the surface. It should be noted that all these processes are dynamic and that their rate changes significantly with time. All these possible processes point to the idea that the In particles may remain trapped in the pores of oxide film, and accordingly may increase its resistance, which was proved by impedance measurements.

At the end of the measurement, a thick grey layer of corrosion products, that completely covers the surface of electrode, can be seen by naked eye. After removing this layer, the surface of Al–In–Sn alloy exhibited rough morphology that is consistent with strong general dissolution (Fig. 5d).

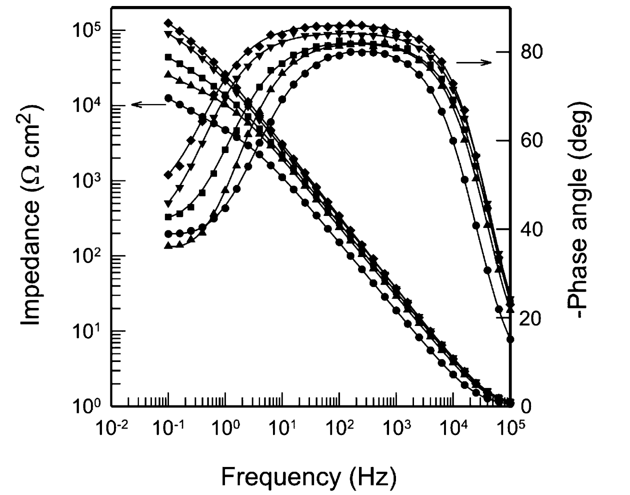

Fig. 6. Bode plots for Al electrode exposed to 2 M NaCl solution for: (●) 0 h, (▲) 2 h, (■) 4 h, (▼) 24 h and (♦) 72 h.

3.3. Impedance measurements

In order to obtain a physical image of the observed systems and to explain all observed phenomena during the 17 days stabilization of Al and its alloys at open circuit potential impedance measurements have been performed. The potentials which established during the stabilization, and at which impedance spectra were recorded, are shown in Fig. 3.

Fig. 6 shows a Bode plots (logarithm of impedance, Z, and phase angle, respectively, vs. logarithm of frequency, f) obtained for the Al electrode after various exposure times up to 3 days in a NaCl solution. At high frequencies (f > 10 kHz) the data are dominated by electrolyte resistance. In the medium frequency region the slope of the log $|Z|$ vs. log f curve close to -1 and the phase angle of $\approx -80^\circ$ determined the capacitive behavior of the system. At the lowest frequencies, the phase angle of $\approx -40^\circ$ and slope of the log $|Z|$ vs. log f close to -0.5 pointed out on the presence of diffusion controlling process. It can be seen that the overall impedance of system increases with time, which indicates that the electrode surface gets more protection.

The development of more than one time constant is deduced from the inspection of the spectra, which reflect the diversity of the phenomena, which occur in the system under investigation. The first time constant, observed in the high frequency region is generally associated with dielectric properties of surface oxide film while the second time constant, observed in the low frequency region, is associated with the diffusion process in oxide film and clearly indicated that mass transport occurring through the phase layer must be taken into account by describing metal/oxide film/electrolyte interfaces.

The results obtained can be described best by equivalent circuit shown in Fig. 7, involving the elements R_{el}, Q_1, R_1 and Q_2. In this circuit the R terms represent resistor elements, while the Q terms represent constant phase elements (CPE). The constant phase element is used to describe the distribution of relaxation times, as a

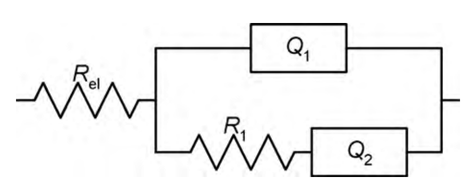

Fig. 7. Equivalent circuit employed in the fitting analysis of the impedance diagrams for Al and Al–In alloy.

Table 1
Electrochemical parameters obtained by fitting analysis of impedance diagrams of Al electrode using the $R_{el}(Q_1(R_1Q_2))$ equivalent circuit.

t (h)	$Q_1 \times 10^6$ (Ω^{-1} s^n cm^{-2})	n_1	R_1 (kΩ cm^2)	$Q_2 \times 10^6$ (Ω^{-1} s^n cm^{-2})	n_2
0	18.71	0.91	3.85	114.56	0.48
1	12.82	0.90	7.99	84.63	0.49
2	10.99	0.92	12.65	68.63	0.51
3	10.19	0.92	17.03	59.96	0.50
4	9.74	0.92	21.02	33.72	0.51
24	7.29	0.94	59.29	16.21	0.47
48	6.51	0.96	80.03	13.01	0.48
72	6.06	0.96	84.76	10.45	0.52
96	9.43	0.95	70.94	21.46	0.51
168	20.21	0.92	27.75	143.51	0.51
192	24.78	0.91	23.06	180.39	0.49
216	28.99	0.90	19.28	227.36	0.47
240	32.48	0.86	16.79	288.72	0.48
264	37.43	0.85	13.56	326.49	0.49
336	54.93	0.82	7.99	621.55	0.52
360	57.21	0.82	7.01	784.43	0.51
384	59.97	0.80	6.63	916.77	0.51
408	64.52	0.81	5.68	1074.48	0.50

result of inhomogenities present at the solid/liquid interface on a microscopic level. Its impedance, Z_{CPE}, is described by expression $Z_{CPE} = [Q(j\omega)^n]^{-1}$ [44], where the constant Q accounts for a combination of properties related to both the surface and the electroactive species, $j\omega$ is the complex variable for sinusoidal perturbation with $\omega = 2\pi f$ and n is the exponent of CPE. The parameter n is also a constant that can assume different values in the range from -1 to +1. When the value of n approaches unity the CPE is equivalent to a capacitor, while n values close to 0.5 are indicative of diffusion, and consequently the CPE represents a Warburg diffusion component. Furthermore, for n values close to 0 the CPE represents the resistance and for n close to -1, an inductance.

According to the fitting results, the n values for Q_1 are about 0.9, whale the n values for Q_2 are close to 0.5. Hence, in equivalent circuit shown in Fig. 7, Q_1 is a constant phase element (CPE) accounts for the oxide film and double layer capacitances (in series) while Q_2 represents a Warburg diffusion process in the oxide film and R_1 is the charge transfer resistance. R_{el} corresponds to the electrolyte resistance and was found to be in the order of 1 Ω cm^2. Numerical values for each individual element of the equivalent circuit for Al as a function of immersion time are shown in Table 1.

It can be seen that the charge transfer resistance (R_1) increased, while the capacity of phase boundary (Q_1), and the diffusion element (Q_2) decreased with immersion time up to 3 days. This direction of change is attributed to the increase of protective properties of the surface layer on the electrode. Furthermore, according to the plate capacitor model the oxide film capacity, C, is inversely proportional to its thickness, d (according $C = \varepsilon_0\varepsilon/d$; ε_0 is the permittivity of vacuum, ε is the relative permittivity of the film). Hence, the reduction of Q_1 with the increase of immersion time up to 3 days matches the corresponding increase of the thickness of the surface layer, which additionally indicated on increase of protective properties of the oxide layer at the surface of the Al.

The electrochemical and corrosion behavior of Al greatly depends on the specific activity of the present ions, especially anions (OH^- and Cl^- ions). Namely, two processes occur simultaneously at the oxide/electrolyte interface upon stabilization of electrodes at the open circuit potential: adsorption of OH^- ions and adsorption of Cl^- ions. Adsorption of OH^- and Cl^- ions at the surface of Al is a dynamic process that depends on various factors, of which time, purity of Al (alloying element) and state of surface are the most important. While, in the first place, the adsorption of OH^- ions leads to sample passivation and to improvement of the properties of the protective oxide layer on the surface of Al, adsorption of Cl^- ions can lead to depassivation of Al, that is to a local dissolution of Al. Chloride ion adsorption generally occurs at oxides' defects, such as minor cuts, dips, cracks, or pores, that is where the oxide thickness is smaller, and electric field is stronger [45–48]. This phenomenon can cause significant changes in the charge transfer as is happening in the inner, the so called Helmholtz part, of the electrochemical double layer. The depassivation time corresponds to time in which the amount of adsorbed aggressive ions is enough to cause nucleation of local dissolution of Al. In the overall process of dissolution, the slow stage is oxide dissolution with creation of soluble salts with cations from the oxide lattice. Pits created continue to activate local dissolution by autocatalytic process. In the pit, there is a high concentration of metal chlorides (M^+Cl^-) and as a result of hydrolysis, a high concentration of H^+ ions. Both H^+ ions and Cl^- ions stimulate the dissolution of metal, and the entire process accelerates with time. Thus, pits propagate as a consequence of the reduction of pH within the pit [49].

It was really found out that at longer exposure times i.e. after 3 days, there is a fall in the modulus of parameter R_1 and an increase of the parameters Q_1 and Q_2, while a general shape of impedance diagram is maintained (Fig. 8, Table 1). This direction of change is attributed to the penetration of the oxide film by chloride ions. These conditions favour the development of pitting corrosion on the surface of Al, which was confirmed by optical microscopy examination (Fig. 5a).

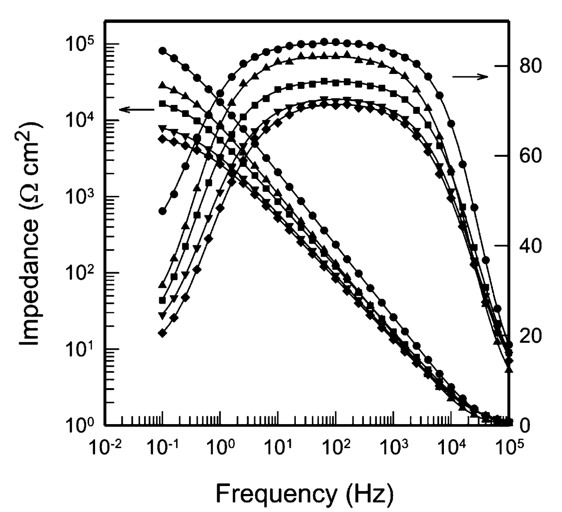

Fig. 8. Bode plots for Al electrode exposed to 2 M NaCl solution for: (●) 96 h, (▲) 168 h, (■) 240 h, (▼) 336 h and (♦) 408 h.

Table 2
Electrochemical parameters obtained by fitting analysis of impedance diagrams of Al–In alloy using the $R_{el}(Q_1(R_1Q_2))$ equivalent circuit.

t (h)	$Q_1 \times 10^6$ (Ω^{-1} s^n cm^{-2})	n_1	R_1 (Ω cm^2)	$Q_2 \times 10^6$ (Ω^{-1} s^n cm^{-2})	n_2
0	21.64	0.91	603.21	432.94	0.48
1	17.01	0.91	622.19	413.49	0.47
2	14.25	0.92	666.73	394.87	0.50
3	12.48	0.93	685.46	376.75	0.52
4	11.08	0.93	738.92	361.34	0.51
24	8.64	0.94	857.56	270.58	0.48
48	7.79	0.94	988.42	209.72	0.49
72	12.72	0.94	896.57	287.58	0.50
96	14.38	0.93	800.99	346.38	0.51
168	27.21	0.91	590.19	448.55	0.52
192	31.01	0.89	546.53	491.07	0.50
216	35.79	0.88	496.71	567.78	0.46
240	40.17	0.85	469.98	648.21	0.47
264	52.56	0.84	378.16	737.79	0.49
336	83.47	0.83	354.11	1006.53	0.49
360	94.09	0.83	337.67	1099.47	0.52
384	106.95	0.80	310.27	1176.11	0.50
408	127.31	0.81	299.16	1243.68	0.48

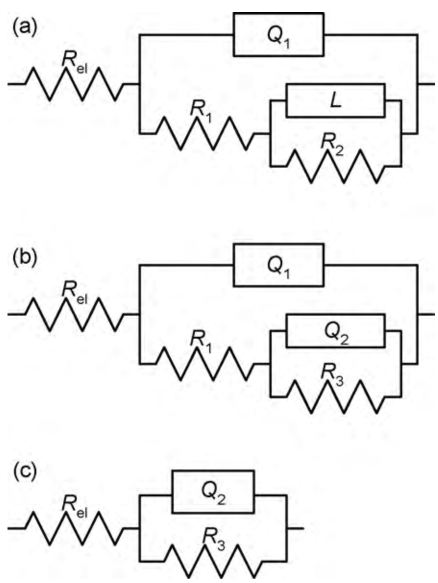

Fig. 9. Equivalent circuits employed in the fitting analysis of the impedance diagrams for Al–Sn and Al–In–Sn alloys: (a) for 0 and 1 h, (b) for 2, 3 and 4 h and (c) for $t \geq 24$ h.

In contrast to aluminium, Al–In alloy shows greatly active behavior. During the first 2 days an increase of impedance is evident, after which the tendency is reverse, indicating that the corrosion process is beginning. The obtained impedance spectra have been interpreted according to the equivalent circuit shown in Fig. 7. The corresponding fitting results are listed in Table 2.

Indium as alloying element in Al enhances the adsorption of Cl^- ions, and hence dissolution of alloy, which is accompanied by a significant decrease in value of R_1, and increase in values of parameters Q_1 and Q_2. It can be seen that, after 17 days, the oxide film doesn't show any protective properties and the significant surface damage was observed, mainly at the grain boundaries were the indium inclusions are located (Fig. 5b).

The impedance spectra when the Al–Sn and Al–In–Sn alloys are exposed to aggressive NaCl media reveal a different behavior compared to that of technical grade Al. Namely, immediately after immersion tested alloys in solution the appearance of corrosion was evident through the evolution of small bubbles of hydrogen. With continued corrosion the materials lost their reflective surface and the thick layer of corrosion products is formed. Impedance measurements confirmed this visual observation. The impedance parameters were determined using the equivalent electrical circuit models presented in Fig. 9a–c.

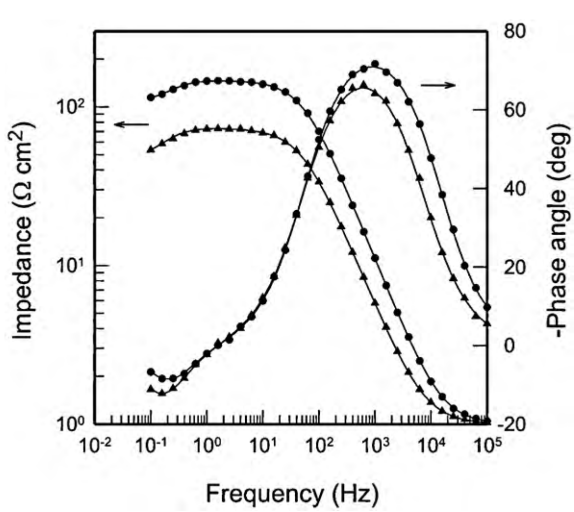

Fig. 10. Bode plots for Al–Sn alloy exposed to 2 M NaCl solution for: (●) 0 h and (▲) 1 h.

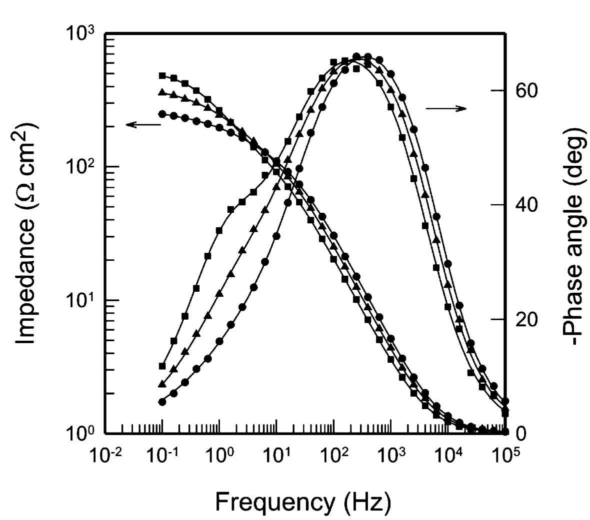

Fig. 11. Bode plots for Al-Sn alloy exposed to 2 M NaCl for: (●) 2 h, (▲) 3 h and (■) 4 h.

Table 3
Electrochemical parameters obtained by fitting analysis of impedance diagrams of Al–Sn alloy.

t (h)	Equivalent circuit	$Q_1 \times 10^6$ (Ω^{-1} s^n cm^{-2})	n_1	R_1 (Ω cm^2)	L (H cm^2)	R_2 (Ω cm^2)	$Q_2 \times 10^6$ (Ω^{-1} s^n cm^{-2})	n_2	R_3 (Ω cm^2)
0	$R_{el}(Q_1(R_1(LR_2)))$	37.97	0.89	106.57	25.18	39.75			
1	$R_{el}(Q_1(R_1(LR_2)))$	89.51	0.87	46.39	20.46	26.32			
2	$R_{el}(Q_1(R_1(Q_2R_3)))$	134.04	0.84	117.86			2013.36	0.54	154.11
3	$R_{el}(Q_1(R_1(Q_2R_3)))$	177.23	0.83	131.62			1204.27	0.61	268.39
4	$R_{el}(Q_1(R_1(Q_2R_3)))$	241.36	0.82	150.47			836.34	0.76	385.13
24	$R_{el}(Q_2R_3)$						142.00	0.91	1314.10
48	$R_{el}(Q_2R_3)$						128.01	0.91	2283.42
72	$R_{el}(Q_2R_3)$						120.83	0.92	3624.56
96	$R_{el}(Q_2R_3)$						115.66	0.91	4129.89
168	$R_{el}(Q_2R_3)$						104.15	0.91	6957.68
192	$R_{el}(Q_2R_3)$						98.57	0.90	8162.13
216	$R_{el}(Q_2R_3)$						96.13	0.92	9284.79
240	$R_{el}(Q_2R_3)$						94.87	0.91	10490.78
264	$R_{el}(Q_2R_3)$						91.55	0.91	11741.44
336	$R_{el}(Q_2R_3)$						90.00	0.91	13898.39
360	$R_{el}(Q_2R_3)$						88.74	0.92	14571.94
384	$R_{el}(Q_2R_3)$						87.11	0.92	15091.11
408	$R_{el}(Q_2R_3)$						86.23	0.92	15593.46

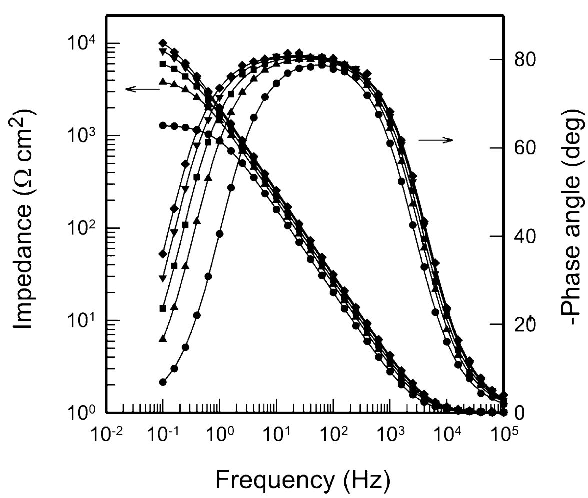

Fig. 12. Bode plots for Al–Sn alloy exposed to 2 M NaCl for: (●) 24 h, (▲) 96 h, (■) 168 h, (▼) 240 h and (♦) 336 h.

As an example, Figs. 10–12 illustrate the change of the impedance spectra for Al–Sn alloy which occurs with increasing exposure time. Through the first hour, the response of Al–Sn alloy in the complex impedance plane (Fig. 9) deviates from the usual behavior, and together with high frequency capacitive time constant an inductive time constant at low frequencies are observed. Similar results are obtained for Al–In–Sn alloy.

It should be noted that the origin of the inductive loop at low frequency is not clear. Numerous examples of such inductive arcs are found in corrosion studies of Al and its alloy, and various explanations for them have been suggested, mainly involving potential-dependent adsorption phenomena of the intermediate or electrically active species or pitting phenomena due to surface area modulation or salt film property modulation [50–52]. One of the most acceptable explanations is given by Mansfeld and associates [53,54]. According to them, the inductive time constant in complex impedance plane can be attributed to the pitting phenomena, at short exposure times, when the values of corrosion and pitting potentials are similar. Namely, as the pitting potential and corrosion potential are nearly the same (in the case of Al–Sn and Al–In–Sn alloys, Fig. 2), even a small increase of the potential above corrosion potential will lead to the initiation and acceleration of pitting with a large increase of the anodic current density [53,54]. In this case, the measured impedance will no longer be the ratio of two sinusoidal signals with the same frequency and different amplitudes and phases, but will be due to a non-linear signal [53,54], which is considered to be reason for the inductive behavior shown in Fig. 10.

Impedance plots have been interpreted according to the equivalent circuit shown in Fig. 9a, in which Q_1 corresponds to the double layer capacity, R_1 to the charge transfer resistance, while components L and R_2 are introduced to describe the inductive behavior of

Table 4
Electrochemical parameters obtained by fitting analysis of impedance diagrams of Al–In–Sn alloy.

t (h)	Equivalent circuit	$Q_1 \times 10^6$ (Ω^{-1} s^n cm^{-2})	n_1	R_1 (Ω cm^2)	L (H cm^2)	R_2 (Ω cm^2)	$Q_2 \times 10^6$ (Ω^{-1} s^n cm^{-2})	n_2	R_3 (Ω cm^2)
0	$R_{el}(Q_1(R_1(LR_2)))$	42.13	0.88	120.15	23.36	46.93			
1	$R_{el}(Q_1(R_1(LR_2)))$	90.21	0.85	80.39	21.15	30.77			
2	$R_{el}(Q_1(R_1(Q_2R_3)))$	126.48	0.84	224.87			1438.15	0.58	282.65
3	$R_{el}(Q_1(R_1(Q_2R_3)))$	160.27	0.84	245.13			873.47	0.66	454.46
4	$R_{el}(Q_1(R_1(Q_2R_3)))$	216.67	0.83	283.67			531.58	0.79	689.51
24	$R_{el}(Q_2R_3)$						127.74	0.92	4501.28
48	$R_{el}(Q_2R_3)$						82.38	0.92	14252.37
72	$R_{el}(Q_2R_3)$						58.94	0.93	21003.48
96	$R_{el}(Q_2R_3)$						53.02	0.93	28084.16
168	$R_{el}(Q_2R_3)$						46.26	0.92	47578.33
192	$R_{el}(Q_2R_3)$						45.84	0.92	51162.97
216	$R_{el}(Q_2R_3)$						45.12	0.92	53253.52
240	$R_{el}(Q_2R_3)$						44.08	0.92	56910.44
264	$R_{el}(Q_2R_3)$						43.78	0.91	58578.29
336	$R_{el}(Q_2R_3)$						40.46	0.92	61909.17
360	$R_{el}(Q_2R_3)$						39.58	0.92	63748.56
384	$R_{el}(Q_2R_3)$						39.20	0.93	64750.83
408	$R_{el}(Q_2R_3)$						37.98	0.93	64664.67

examined systems. The obtained results are listed in Tables 3 and 4. After 1 h a rapid dissolution of the electrodes is confirmed by low values of R_1 and R_2.

However, at longer exposure time, i.e. at $t \geq 2$ h the impedance of Al–Sn (Fig. 11) and Al–In–Sn alloys increase, while in the low frequency range inductive time constant disappears, and another capacitive time constant appears, which can be attributed to some kind of passivity due to formation of film of corrosion products on the surface. In this case the data are analyzed using the equivalent circuit shown in Fig. 9b, in which Q_1 corresponds to the double layer capacity, R_1 to the charge transfer resistance, while additional Q_2 R_3 couple corresponds to the second time constant at the low frequencies, appears to be connected with the presence of the corrosion products film. The obtained values are presented in Tables 3 and 4.

Over time, an amount of oxide accumulates on the surface of the metal increases, the oxide layer becomes thicker and more resistant, and the capacitive time constant, which describes it, grows. After some time (1 day) the system behavior, in the impedance diagram, is completely determined by the passive layer on the electrode surface (Fig. 12). In this case the measurement results can be described by simple equivalent circuit shown in Fig. 9c, and the equivalent circuit parameters for both alloys are listed in Tables 3 and 4. It is evident that the impedance of the Al–Sn and Al–In–Sn alloys increases over time, that is the resistance, R_3, and the thickness of the surface layer increase (i.e., the capacity of the layer, Q_2, reduces). These changes are attributed to the improvement of protective properties of oxide layer on the surface of the investigated alloys. It can also be noted that the surface layer of the Al–In–Sn alloy has better properties than the one of Al–Sn alloy, which is most likely due to incorporation of indium in the pores and defects in the oxide layer.

4. Conclusion

The corrosion behavior of Al, Al–In, Al–Sn and Al–In–Sn alloys in 2 M NaCl solution has been studied by using polarization, open circuit potential, hydrogen collection and impedance measurements as well as by optical microscopy examination. The findings of the present work may be summarized as follows:

- Polarization measurements indicated that the alloying elements considerably change the electrochemical behavior of aluminium. Changes are especially pronounced in the anodic branch of the polarization curve, and manifest in significant shift of the corrosion and the pitting potentials in the negative direction, reducing the passive potential region, and increasing the current output already at low anodic overpotentials.
- The corrosion of aluminium and its alloys is accompanied by the cathodic reaction of hydrogen evolution. The volume of evolved hydrogen increased with time. The obtained results show that the indium inhibits cathodic reaction of hydrogen evolution, while tin catalyzes the same one.
- Corrosion of aluminium alloys occurs by micro-galvanic cells that were established between aluminium and the alloying element. Indium and tin inclusions display a cathodic behavior with respect to the aluminium matrix and hydrogen evolution reaction takes place over these. Acting as cathodic centres, indium and tin inclusions support the dissolution of the surrounding aluminium substrate.
- In this case of Al–In–Sn alloy, the contact of indium and tin lead to the formation of additional micro-galvanic cells in which indium has anodic character in respect to the tin. Therefore, in the first moments of exposure to chloride solution, the dissolution of Al–In–Sn alloy introduces both aluminium and indium ions into the solution. However, the indium species redeposit on the cathodic sits of the surface, subsequently, and caused the hydrogen evolution decrease. In parallel, the oxidation of the metal matrix, the oxide film is formed, which suppresses further anodic dissolution of alloy.
- Impedance measurement performed also during the 17 days of corrosion test provided a continuous monitoring of the parameters which characterize the properties of the surface and their changes as corrosion occurs.
- Microscopy, open circuit potential, hydrogen collection and impedance measurements were complementary in characterization of corrosion behavior of aluminium and its alloys.

References

[1] M. Pourbaix, Atlas of Electrochemical Equilibria in Aqueous Solutions, NACE International Cebelcor, Houston, 1974.
[2] D.S. Keir, M.J. Pryor, P.R. Sperry, J. Electrochem. Soc. 114 (1967) 777; D.S. Keir, M.J. Pryor, P.R. Sperry, J. Electrochem. Soc. 116 (1969) 319.
[3] A.R. Despić, D.M. Dražić, M.M. Perunović, N. Ciković, J. Appl. Electrochem. 6 (1976) 572.
[4] S. Zečević, L. Gajić, A.R. Despić, D.M. Dražić, Electrochim. Acta 26 (1981) 1625.
[5] A. Mance, D. Cerović, A. Mihajlović, J. Appl. Electrochem. 14 (1984) 459.
[6] M.C. Reboul, P.H. Gimenez, J.J. Rameau, Corrosion 40 (1984) 366.
[7] C.D.S. Tuck, J.A. Hunter, G.M. Scamans, J. Electrochem. Soc. 134 (1987) 2970.
[8] D.D. Macdonald, S. Real, M. Urquidi-Macdonald, J. Electrochem. Soc. 135 (1988) 2397.
[9] S.B. Saidman, S.G. Garcia, J.B. Bessone, J. Appl. Electrochem. 25 (1995) 252.
[10] A. Venugopal, R.D. Angal, V.S. Raja, Corrosion 52 (1996) 138.
[11] A. Barbucci, G. Cerisola, G. Bruzzone, A. Saccone, Electrochim. Acta 42 (1997) 2369.
[12] D.R. Salinas, S.G. Garcia, J.B. Bessone, J. Appl. Electrochem. 29 (1999) 1063.
[13] H.A. El Shayeb, F.M. Abd El Wahab, S. Zein El Abedin, J. Appl. Electrochem. 29 (1999) 473.
[14] J. Mathiyarasu, L.C. Nehru, P. Subramanian, N. Palaniswamy, N.S. Rengaswamy, Anti-Corros. Methods Mater. 48 (2001) 324.
[15] Q. Li, N.J. Bjerrum, J. Power Sources 110 (2002) 1.
[16] S. Zein El Abedin, A.O. Saleh, J. Appl. Electrochem. 34 (2004) 331.
[17] Yu.Ya. Andreev, A.V. Goncharov, Electrochim. Acta 50 (2005) 2629.
[18] S. Gudić, J. Radošević, I. Smoljko, M. Kliškić, Electrochim. Acta 50 (2005) 5624.
[19] A.Z. Zhuk, A.E. Sheindlin, B.V. Kleymenov, E.I. Shkolnikov, M.Y. Lopatin, J. Power Sources 157 (2006) 921.
[20] M. Nestoridi, D. Pletcher, R. Wood, S. Wang, R. Jonees, K. Stokes, I. Wilcock, J. Power Sources 178 (2008) 445.
[21] W.M. Carroll, C.B. Breslin, Corros. Sci. 33 (1992) 1161.
[22] J.F. Equey, S. Muller, J. Desilvestro, O. Haas, J. Electrochem. Soc. 139 (1992) 1499.
[23] C.B. Breslin, W.M. Carroll, Corros. Sci. 34 (1993) 1099.
[24] S.B. Saidman, J.B. Bessone, Electrochim. Acta 42 (1997) 413.
[25] A. Venugopal, V.S. Raja, Corros. Sci. 39 (1997) 1285; A. Venugopal, V.S. Raja, Corros. Sci. 39 (1997) 2053.
[26] C.B. Breslin, A.L. Rudd, Corros. Sci. 42 (2000) 1023.
[27] H.A. El Shayeb, F.M. Abd El Wahab, S. Zein El Abedin, Corros. Sci. 43 (2001) 643; H.A. El Shayeb, F.M. Abd El Wahab, S. Zein El Abedin, Corros. Sci. 43 (2001) 655.
[28] J.O'M. Bockris, A.K.N. Reddy, Modern Electrochemistry, vol. 2, Plenum Press, New York, 1974, p. 862.
[29] G.T. Burstein, R.T. Cinderey, Corros. Sci. 33 (1992) 573.
[30] Z. Szklarska-Smialowska, Corros. Sci. 41 (1999) 1743.
[31] S.-M. Moon, S.-I. Pyun, J. Solid State Electrochem. 4 (2000) 267.
[32] R. Parsons, Handbook of Electrochemical Constants, Butterworth, London, 1959.
[33] J.T.B. Gundersen, A. Aytac, J.H. Nordlien, K. Nisancioglu, Corros. Sci. 46 (2004) 697.
[34] B. Graver, A. Helvoort, J.C. Walmsley, K. Nisancioglu, Mater. Sci. Forum 519–521 (2006) 673.
[35] B. Graver, A.M. Pedersen, K. Nisancioglu, ECS Trans. 16 (2009) 55.
[36] Z. Szklarska-Smialowska, Corrosion 27 (1971) 223.
[37] Metals Handbook, vol. 13, ASM International, Materials Park, OH, 1987, p. 113.
[38] J.M.C. Mol, J. Mater. Sci. 35 (2000) 1629.
[39] S. Trasatti, J. Electroanal. Chem. 39 (1972) 163.
[40] A.G. Munoz, S.B. Saidman, J.B. Bessone, Corros. Sci. 44 (2002) 2171.
[41] M. Paramasivam, M. Jayachandran, S. Venkatakrishna Iyer, J. Appl. Electrochem. 33 (2003) 303.
[42] P.R. Birkin, M. Nestoridi, D. Pletcher, Electrochim. Acta 54 (2009) 6668.
[43] A.V. Ilyukhina, O.V. Kravchenko, B.M. Bulychev, E.I. Shkolnikov, Int. J. Hydrogen Energy 35 (2010) 1905.
[44] I.D. Raistrick, J.R. Macdonald, D.R. Franceschetti, in: J.R. Macdonald (Ed.), Impedance Spectroscopy, John Wiley & Sons, New York, 1987.
[45] D.M. Dražić, S.K. Zečević, R.T. Atanasoski, A.R. Despić, Electrochim. Acta 28 (1983) 751.
[46] A. Despić, J. Electroanal. Chem. 184 (1985) 401.

[47] J. Radošević, Z. Mentus, A. Đorđević, A. Despić, J. Electroanal. Chem. 193 (1985) 241.
[48] A.R. Despić, D.M. Dražić, Lj. Gajić-Krstajić, J. Electroanal. Soc. 242 (1988) 303.
[49] J.R. Davis (Ed.), Corrosion: Understanding the Basic, ASM International, Materials Park, OH, 2000.
[50] T.R. Beck, Electrochim. Acta 29 (1984) 485;
T.R. Beck, Electrochim. Acta 30 (1985) 725.
[51] J.B. Bessone, D.R. Salinas, C.E. Mayer, M. Ebert, W.J. Lorenz, Electrochim. Acta 37 (1992) 2283.
[52] A.G. Munoz, J.B. Bessone, Corros. Sci. 41 (1999) 1447.
[53] F. Mansfeld, Electrochim. Acta 35 (1990) 1533;
F. Mansfeld, Electrochim. Acta 38 (1993) 1891.
[54] F. Mansfeld, J.C.S. Fernandes, Corrosion. Sci. 34 (1993) 2105.